Full Title: Coding-sequence evolution does not explain divergence in petal anthocyanin pigmentation between *Mimulus luteus* var. *luteus* and *M. l. variegatus*

Short Title: Monkeyflower pigment divergence not associated with coding-sequence evolution

Walker E. Orr[1]
Ji Yang Kim[1]
Tejas Raj[2]
Ellen K. Hom[1]
Ashley E. Person[1]
Anne Vonada[1]
John A. Stratton[2]
Arielle M. Cooley[1,*]

[1]Whitman College Biology Department, Walla Walla WA, 99362, U.S.A.
[2]Whitman College Computer Science Department, Walla Walla WA, 99362, U.S.A.
*Corresponding author

Abstract

Phenotypic transitions in related taxa often share a common genetic basis, which suggests that there are constraints that shape the process of evolution at the genetic level. For example, noncoding changes in a gene may be favored relative to coding changes. Non-coding changes, which can alter context-specific gene expression, tend to have fewer pleiotropic consequences than coding changes, which affect the function of a gene product in all contexts. In this study, we evaluate the importance of coding-sequence changes to the recent evolution of a novel

anthocyanin pigmentation trait in the monkeyflower genus *Mimulus*. The magenta-flowered *Mimulus luteus* var. *variegatus* recently gained petal lobe anthocyanin pigmentation via a single-locus Mendelian difference from its sister taxon, the yellow-flowered *M. l. luteus*. Mapping and functional tests previously showed that transcription factor *MYB5a/NEGAN* is the single gene responsible for this difference. We overexpressed the genomically encoded protein-coding sequences of *MYB5a*, from both *M. l. luteus* and *M. l. variegatus*, in *Nicotiana tabacum* leaves, in order to test their efficacy as anthocyanin-pigment activators. Quantitative image analysis of transfected tobacco leaves revealed robust anthocyanin production driven by both types of transgenes, compared to a negative control, and overall functional equivalency between the *luteus* and *variegatus* alleles. This finding supports the hypothesis that petal pigment was not gained by protein-coding changes in *M. l. variegatus*, but instead via non-coding *cis*-regulatory evolution. While constructing the transgenes needed for this experiment, we unexpectedly discovered two sites in *MYB5a* that appear to be post-transcriptionally edited – a phenomenon that has been rarely reported, and even less often explored, for nuclear-encoded plant mRNAs.

Keywords: anthocyanin regulation; floral color patterning; gene expression; *cis*-regulatory evolution; R2R3 MYBs; *Mimulus*; petal lobe pigmentation; post-transcriptional mRNA editing; A-to-I editing; transient transformation; digital image analysis

Introduction

To what extent are the molecular mechanisms of evolutionary diversification predictable? Biologists have long been interested in understanding constraints on the evolutionary process, which can increase our ability to predict the molecular mechanisms that underlie a specific trait. For example, coding and noncoding mutations have been hypothesized to differ in their contributions to evolutionary change (Hoekstra and Coyne, 2007; Stern and Orgogozo, 2008). Noncoding "*cis*-regulatory" regions integrate upstream signals to determine the conditions under

which a protein will be expressed. These regions tend to be organized into modules, and so mutations can easily generate new patterns of gene expression without altering gene product function or existing expression patterns (Wray, 2007). By contrast, a change in a gene's coding sequence tends to be more pleiotropic since it will likely alter the gene product's function in all contexts under which that gene is expressed. Stern and Orgogozo (2008) have proposed a model in which the relative importance of coding and noncoding changes to the evolution of a new function in a gene depends on that gene's function, the selective strength and evolutionary time-scale, and the position of that gene within gene networks. This model predicts that the contribution of coding changes to phenotypic transitions will decline with evolutionary distance between the diverged taxa, due to lower average fitness values for coding changes compared to noncoding changes. The pattern has been documented empirically by Wittkopp et al. (2008) in *Drosophila*.

In plants, transitions in anthocyanin pigmentation are especially well suited to investigating the mechanisms of molecular evolution (Davies et al., 2012; Sobel and Streisfeld, 2013; LaFountain and Yuan, 2021; Li et al., 2022). Anthocyanins are a class of flavonoids that are responsible for purple, pink, and red colors in diverse angiosperm tissues, including leaves, seed coats, and flowers (Durbin et al., 2003). The anthocyanin biosynthetic pathway (ABP) is well-described and conserved across taxa (Feller et al., 2011). Depending on the species, ABP genes are organized into one or two gene batteries. In the model plant *Arabidopsis thaliana*, "early" genes include *CHS, CHI,* and *F3'H*; late genes include *DFR, ANS,* and *UF3GT* (Dubos et al., 2010). Early genes generally encode for enzymes that produce pathway intermediates with diverse fates; these intermediates play important roles in protection against UV radiation, defense against pathogens, signaling, male fertility, and auxin signaling (Koes et al., 2005). Late genes encode enzymes that are responsible for the production of anthocyanins and proanthocyanidins (condensed tannins) from these intermediates.

The "late" gene battery is coordinately regulated by MBW transcription factor complexes. In these complexes, a bHLH protein associates with a WD40 and an R2R3-MYB partner to activate the transcription of several downstream genes in specific tissues (Grotewold, 2006). Much of the target specificity of an MBW complex is conferred by the R2R3-MYB partner in the complex: different tissues make use of different *MYB* genes to stimulate anthocyanin production, but may use the same *bHLH* gene (Quattrocchio et al., 2006). *MYB* genes thus serve as "input-output" integrators that regulate gene batteries under highly specific contexts. Consistent with their position in gene networks and the hypothesized importance of "input-output" genes in repeated evolution events, *MYB* genes demonstrate remarkable reuse in floral pigment transitions across a variety of species (Streisfeld and Rausher, 2011; Yuan et al., 2013).

The independent evolution of petal lobe anthocyanin (PLA) pigmentation in three lineages in the *luteus* group of the monkeyflower genus *Mimulus* (synonym *Erythranthe*; see Barker (2012) and Lowry et al. (2019)) provides an opportunity to test the relative importance of coding and noncoding changes at different evolutionary time-scales (Beardsley and Olmstead, 2002). *Mimulus* lends itself to studies in plant evo-devo, thanks to a diversity of species with short generation times, high fecundity, amenability to greenhouse cultivation, and a large range of environmental adaptation (Wu et al., 2008; Yuan 2018). Sequenced genomes have been published for several species including *M. guttatus* (Puzey et al., 2017) and *M. l. luteus* (Edger et al., 2017).

The *luteus* group of *Mimulus* has an ancestral phenotype of yellow (carotenoid-pigmented) flowers with red (anthocyanin-pigmented) spots in the nectar guide region (Fig. 1). The overall color of the anthocyanin-pigmented petal tissue ranges from orange in *M. cupreus*, to red in *M. l. luteus*, to magenta in *M. l. variegatus* and *M. naiandinus*, depending on the relative intensity of carotenoid and anthocyanin pigmentation (Fig. 1).

In three members of the *luteus* group—the magenta-flowered *M. l. variegatus* and *M. naiandinus,* and the orange-flowered *M. cupreus*—anthocyanin pigment has expanded into the petal lobes. The gain of PLA is a derived, single-locus Mendelian trait in all three taxa. In *M. cupreus* and *M. naiandinus*, this is controlled by the *pla1* locus, which contains candidate anthocyanin-activating genes *MYB2* and *MYB3a* (Cooley et al., 2011). A rare yellow-flowered morph of *M. cupreus* does not bear petal lobe anthocyanins (PLA). Since it is found in a single population in Chile, intermingled with orange morphs of *M. cupreus* (Cooley et al., 2008), it is likely to represent a secondary loss of the PLA trait. The lack of PLA in the yellow morph segregates as a single-locus trait mapping to *pla1*. In *M. l. variegatus*, the gain of PLA is conferred by an unlinked second locus, *pla2*, containing candidate gene *MYB5a/NEGAN*. All of the candidate genes at *pla1* and *pla2* belong to the anthocyanin-activating subgroup 6 of the R2R3 MYB gene family (Cooley et al., 2011).

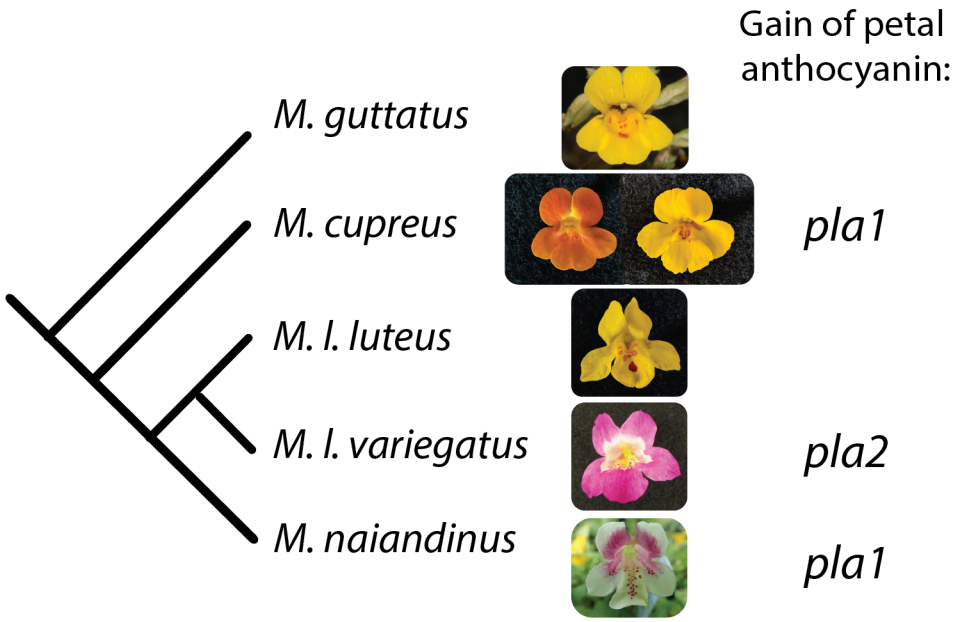

Fig. 1. Petal lobe anthocyanin has been gained repeatedly in the *luteus* group of *Mimulus*. Closely related species outside the *luteus* group, like *M. guttatus*, are typically yellow-flowered, with red anthocyanin

pigmentation restricted to the nectar guide region of the corolla. *Mimulus cupreus* and *M. naiandinus* have each gained petal lobe anthocyanin via a single-locus change at genomic region *pla1*, while the magenta-petaled *M. luteus* var. *variegatus* gained petal lobe anthocyanin via a change at *pla2*. A rare yellow-flowered morph of *M. cupreus*, found in a single population in Chile, has lost petal lobe anthocyanin via a change at *pla1*. Figure modified from Zheng et al. (2021).

While transitions in floral pigment traits have been extensively studied in plants, pigment losses have been investigated more often than pigment gains (Rausher, 2008). Studying the repeated gain of PLA in the *luteus* group presents an opportunity to rectify this. PLA transitions in the group also enable a test of the Stern and Orgogozo (2008) prediction that protein-coding changes are relatively more important within populations, while noncoding changes become increasingly abundant as evolutionary divergence increases. Consistent with this prediction, the rare yellow morph of *M. cupreus* - a within-population polymorphism linked to *pla1* (Cooley and Willis 2009; Cooley et al. 2011) - appears to be associated with a deletion or other major mutation in exon 3 or 4 of *MYB2* (Supplemental Figures S1-S4). Based on the Stern and Orgogozo (2008) model, we expect that the fixed gains of PLA in *M. l. variegatus*, orange *M. cupreus*, and *M. naiandinus*, are more likely to be caused by *cis*-regulatory evolution.

Of the three taxa that have recently gained PLA, *M. l. variegatus* is the most thoroughly characterized. In *M. l. variegatus,* a combination of genetic mapping, *MYB5a* RNAi and overexpression, and transcriptomic studies of wild-type versus *MYB5a* RNAi lines, shows that *MYB5a* is both necessary and sufficient for the gain of PLA (Cooley et al. 2011; Zheng et al., 2021), and points to one particular splice variant of the gene as participating in anthocyanin activation.

Unlike most *MYB* genes, which have a conserved three-exon structure (Dubos et al., 2010), *MYB5a* in *M. l. luteus* and *M. l. variegatus* has four exons. The exon 1-2-4 splice variant, but not the 1-2-3 variant, was found to be abundant specifically in anthocyanin-pigmented petal tissue: the petal lobes of *M. l. variegatus* and the nectar guide regions of both taxa (Zheng et al. 2021). Knockdown of the 1-2-4 splice variant resulted in the loss of petal pigmentation from *M. l. variegatus* (Zheng et al., 2021). Finally, the exon 1-2-4 splice variant of *M. l. variegatus* - but not the 1-2-3 splice variant - contains the subgroup 6 motif found in all known R2R3 MYB anthocyanin activators (Stracke et al., 2001). Thus, the exon 1-2-4 splice variant of *MYB5a* appears to be responsible for the gain of petal lobe anthocyanins in *M. l. variegatus*. While its pattern of spatially specific expression suggests a mechanism of *cis*-regulatory evolution, it is possible that divergence of the protein-coding sequence of *MYB5a* was additionally required for its function in *M. l. variegatus* petal lobe tissue.

In previous studies (Zheng et al., 2021), we relied on the stable transformation procedure published by Yuan et. al. (2013) to test hypotheses about *MYB* gene function. While the method is capable of producing stably transformed offspring, it has the disadvantage of having a low transformation efficiency (about one seed per thousand in *M. l. variegatus*) and a large time cost of about five months between infiltration of native plants and flowering of transformant offspring. Transient transformation is an attractive alternative for more rapid tests of gene function, particularly for genes - such as pigment activators - that are expected to produce an easily visible phenotype. In transient expression, the transgene is delivered to plant cells and transcribed by the plant's transcriptional machinery without necessarily being incorporated into the plant's genome, and transient transformation is regularly used in the tobacco genus *Nicotiana* (Kapila et al., 1997; Schöb et al., 1997; Yang et al. 2000; Sparkes 2006). *Nicotiana* is relatively closely related to *Mimulus*, as the two genera belong to the sister orders of Solanales and Lamiales, respectively, and *Nicotiana* is a highly tractable system for transgenic experimentation. It is

routinely used for heterologous genetic experiments *in planta*, including tests of flower color genes from both rosids and asterids (Montefiori et al., 2015; Tian et al., 2017). Ding and Yuan (2016) adapted methods from *Nicotiana* for use in *Mimulus lewisii*. In our hands, however, transient transformation caused substantial leaf tissue death in both *M. lewisii* and *M. l. luteus*. We therefore returned to *Nicotiana*, using *N. tabacum* as the host for transient tests of *MYB5a* gene function.

If the gain of petal lobe anthocyanin (PLA) in the magenta-flowered *M. l. variegatus* is caused solely by a *cis*-regulatory-driven spatial expansion of *MYB5a* function, then we predict that the coding sequences of *MYB5a* from *M. l. variegatus* and the yellow-flowered *M. l. luteus* will be equally capable of stimulating anthocyanin production. We tested this hypothesis by transiently expressing each taxon's *MYB5a* exon 1-2-4 sequence, as well as a negative control, in leaves of *N. tabacum*. We used a custom image analysis pipeline to rapidly generate quantitative estimates of pigment production in the transformed leaves.

Somewhat surprisingly, the *luteus* allele of *MYB5a* was more often successful than the *variegatus* allele at activating visible quantities of anthocyanin pigmentation in tobacco leaves. However, amongst leaves that did produce visible anthocyanin, the two alleles of this anthocyanin-activating transcription factor were statistically indistinguishable. This indicates functional equivalency of the two sequences, at least in the context of the heterologous tobacco pigmentation pathway, and points to *cis*-regulatory evolution at the causal *MYB5a* gene as a more likely driver of the gain of petal lobe anthocyanin pigmentation in *M. l. variegatus*.

Methods

Plant materials and growth conditions

Nicotiana tabacum cv. Petit Havana SR1 seeds were obtained from Lehle Seeds (Round Rock, TX, USA). *Mimulus lewisii*, line LF10HT1 (two generations inbred) seeds were a gift from the Yao-Wu Yuan lab at the University of Connecticut (Storrs, CT, USA). *Mimulus luteus* var. *luteus* and *M. l. variegatus* were originally collected in Chile from the El Yeso and Río Cipreses populations, respectively (Cooley et al. 2008), and self-fertilized repeatedly with single-seed descent to generate highly inbred lines. In this work, we utilized the 12-generations inbred line *M. l. luteus* EY7 and the 11-generations inbred line *M. l. variegatus* RC6.

Seeds were surface-planted on wet soil and grown at Whitman College (Walla Walla, WA, USA) in a greenhouse with 16-hour day lengths and temperatures ranging from 15ºC to 30ºC. Plants were misted daily and fertilized three times per week with Open Sesame flowering fertilizer (Fox Farm, Samoa, CA, USA).

Determining the genomically encoded sequence of MYB5a *from* M. l. variegatus

While investigating the *MYB5a* protein-coding regions of *M. l. luteus* and *M. l. variegatus*, using the cloning and sequencing methods described in Zheng et al. (2021), we discovered an unexpected new sequence in the fourth exon of *M. l. variegatus Myb5a*. In two different sequencing reactions, originating from two distinct cDNA syntheses from a single mRNA extraction from young bud *M. l. variegatus* tissue, a “GG” variant was found in which adenines at positions 582 and 684 of the exon 1-2-4 splice variant were replaced with guanines (Figure 2). A third sequencing reaction from the same mRNA extraction produced the expected “AA” sequence that was previously reported in Zheng et al. (2021). Because the same two variants were observed, twice each, in the same two samples, we discounted the likelihood of four random sequencing errors. Instead, we hypothesized that the “GG” variant might be encoded in

the genome of *M. l. variegatus*, perhaps representing an alternate allele of *MYB5a* or a closely related gene duplicate, or that it might be the result of post-transcriptional editing.

To determine whether the "GG" variant represented the genomic sequence of an unknown, related *MYB* gene, we cloned and sequenced a fragment of genomic *MYB5a* from an F1 hybrid of *M. l. luteus* x *M. l. variegatus* using primers Myb5_64F and Myb5_57R (Supplemental Table S1), which encompass the first of the two sites in question; these primers were selected because they reliably amplified *MYB5a* from both *M. l. luteus* and *M. l. variegatus*. We reasoned that, if the "GG" variant were from a paralogous *MYB* gene, then we should be able to recover both variants from the F1 hybrid. The "AA" variant would originate from the *M. l. variegatus* *MYB5a* and the "GG" variant would originate from the other, unknown gene; we would also expect to recover the *M. l. luteus* allele of *MYB5a*. If the "GG" variant instead represented residual heterozygosity in *M. l. variegatus*, or post-transcriptional editing of the mRNA, then any single F1 hybrid would contain only one of the two *M. l. variegatus* variants, along with the *M. l. luteus* allele of *MYB5a*.

To determine whether the "GG" variant represented genomically encoded, residual heterozygosity in our highly inbred *M. l. variegatus*, we similarly cloned and sequenced genomic *MYB5a* from the *M. l. variegatus* inbred line. If the "GG" variant were the result of post-transcriptional modification, it should be absent from all genomic DNA samples (both the F1 hybrid and the *M. l. variegatus*).

Finally, to determine whether the "GG" variant could be repeatably isolated from cDNA, we performed new mRNA extractions, and cloned and sequenced *MYB5a* cDNA, from two types of *M. l. variegatus* and *M. l. luteus* floral tissues: the nectar guide region, which is anthocyanin-pigmented in both taxa, and the petal lobe region, which is anthocyanin-pigmented only in *M. l.*

variegatus. Because exons 3 and 4 are partial duplicates of each other, primers Myb5_64F and Myb5_57R (Supplemental Table S1) amplified both splice variants (exon 1-2-3 and 1-2-4) from *M. l. luteus*, though only the exon 1-2-4 variant from *M. l. variegatus*. See Supplemental Figure S5 for an illustration of primer binding sites for both taxa.

Figure 2. Putative A-to-I editing sites in the exon 1-2-4 splice variant of *M. l. variegatus MYB5a*. A. Dark gray bars show the exon structure from start codon to stop codon. Light gray bars show the DNA-binding R2 and R3 domains common to all members of the R2R3 MYB gene family (Stracke et al. 2001). "Subgroup 6" is a sequence motif that is conserved across all R2R3 MYB genes that encode activators of anthocyanin biosynthesis (Stracke et al. 2001). The two putative A-to-I editing sites are each marked as "edited site". B. Chromatograms from *MYB5a* Variant AA and Variant GG. The two polymorphic sites are both located in the fourth exon of *MYB5*, 584 and 686 nucleotides downstream of the translation start site. Nucleotide and amino acid differences are highlighted. Sequences were obtained using Sanger sequencing and were visualized using Geneious R10.

265

266 *Nucleic acid extraction, PCR, and cloning*

267

268 Genomic DNA was extracted from young leaves and floral buds using the Zyppy DNeasy
269 Extraction kit (Zymo Research, CA, USA) according to the manufacturers' protocol. RNA was
270 extracted from buds using the E.Z.N.A. Plant RNA Kit (Omega Bio-Tek, GA, USA) with the
271 DNAse I digestion protocol added to it. cDNA was synthesized using the qScriptTM cDNA
272 Synthesis Kit (Quanta BioSciences, Inc., MD, USA). Quality and concentration of DNA and RNA
273 were quantified using a nanodrop.

274 Fragments of *MYB5a* spanning one or both adenine/guanine polymorphic sites were PCR
275 amplified using the primers listed in Table S1 with G-Biosciences Taq polymerase (St. Louis,
276 MO, USA). Reactions were run with 10μM forward and reverse primers, G-Biosciences 10x
277 buffer, and 2.5μM dNTPs. Annealing temperatures were set to 3℃ below the primer's lowest
278 melting temperature and the number of PCR cycles ranged from 30-32.

279 PCR products were purified and cloned into pGEM vectors in *E. coli* as described in Zheng et al.
280 (2021). Colonies were PCR-screened for inserts of the correct size using primers M13F(-20)
281 and M13R(-24). Sanger sequencing was performed by Eton Biosciences (San Diego, CA, USA)
282 and sequences were visualized using Geneious R9 and R10.

283

284 *Strategy for testing for functional equivalence of two coding sequences*

285

286 Once the "AA" allele had been identified as the only genomically encoded *MYB5a* sequence
287 present in the magenta-flowered *M. l. variegatus*, transgenes were constructed to test whether
288 the exon 1-2-4 splice variant was functionally equivalent to the corresponding allele from the
289 yellow-flowered *M. l. luteus* (which lacks petal lobe anthocyanins), as described below. Each

transgene, as well as a negative control, was transfected into leaves of *Nicotiana tabacum*, and the area of the spot of anthocyanin pigment produced following each infiltration was quantified. The heterologous *N. tabacum* system was selected because our pilot studies in *M. l. luteus* and another monkeyflower species, *M. lewisii*, failed to produce visible anthocyanin pigment.

Bacterial culturing for transgene construction

Escherichia coli cultures were grown at 37ºC in Luria-Bertani (LB) broth: 10g/L tryptone, 5g/L yeast extract, 10g/L NaCl in demineralized water, sterilized by autoclaving. *Agrobacterium tumefaciens* cultures were grown at 28 ºC in LB broth with the NaCl concentration reduced from 10g/L to 5g/L.

Cells containing plasmids with a Kanamycin-resistance gene were grown in media containing 50 µg/mL kanamycin. The *A. tumefaciens* strain, GV3101, used in these studies contains gentamicin- and rifampicin-resistance genes; these cultures were grown in media additionally containing 50 µg/mL gentamicin and 25 µg/mL rifampicin. Liquid cultures were grown at the appropriate temperature with shaking at 200 rpm. To isolate individual colonies, cells were grown on plates containing LB media with appropriate selective antibiotics and 15 g/L agar.

Construction of Gateway® Entry Vectors

The exon 1-2-4 splice variant of *MYB5a* was amplified from *M. l. variegatus* petal cDNA, using primers cacc10F and Myb5_69R (Supplemental Table S1) and New England Biolabs® Phusion® High-Fidelity DNA Polymerase. Amplicons were transformed into the pEARLEYGATE101 Gateway vector (Earley et al. 2006). From there, the coding sequence without a stop codon was

315 amplified from plasmid DNA containing *M. l. variegatus MYB5a* CDS using the same primers and
316 polymerase.
317
318 The pENTR-D/TOPO Cloning Kit was used to produce directionally-cloned Gateway® entry
319 clones carrying *M. l. variegatus MYB5a* CDS. The reaction mixture was transformed into TOP10™
320 *E. coli* cells, and colonies were screened for the presence of the insert via PCR, using the
321 Myb5_10F, M13R(-24) primer pair. Three colonies that gave a band at ~1-kb were selected for
322 sequencing. The M13F(-20), M13R(-24) primer pair was used to amplify and sequence the insert.
323 Sanger sequencing was performed by Eton BioScience® (San Diego, CA, USA) and checked for
324 errors against reference sequence in Geneious® version 9.1.8 (https://www.geneious.com).
325
326 For *M. l. luteus*, amplification of the exon 1-2-4 splice variant was attempted without success using
327 cDNA extracted from young bud tissue of *M. l. luteus* lines EY1 and EY7. *M. l. luteus* EY7 is
328 known to express *MYB5a* in the anthocyanin-spotted nectar guide region of the flower bud, but
329 expression levels are low (Zheng et al. 2021). Instead, this protein-coding region was synthesized
330 by GENEWIZ (Plainfield, NJ, USA) based on the published genomic sequence of *M. l. luteus*
331 (Edger et al., 2017). The sequence was delivered in a pUC57 vector, but with attL1 and attL2
332 homology sites added to the 5'- and 3'- ends of the gene, respectively, to facilitate Gateway
333 recombination. Upon receipt, the plasmid was transformed into TOP10™ chemically competent
334 *E. coli* cells, and colonies were screened for the presence of the insert via PCR, using Myb5_12F
335 internal forward primer and M13R(-24) reverse primer (primer table). Sanger sequencing was
336 performed by Eton BioScience, and sequence was checked for errors against the reference
337 sequence in Geneious.
338
339 *Construction of Gateway® Plant Expression Vectors*
340

The LR Clonase II kit (ThermoFisher Scientific, Waltham, MA, USA) was used to transfer each insert from an entry vector to destination vector pEARLEYGATE101 (Earley et al. 2006). Entry vectors used in this study were pENTR with *M.l.variegatus MYB5a* CDS and pUC57 with *M.l.luteus MYB5a* CDS.

Reactions were transformed into TOP10™ chemically competent *E. coli* and screened for the presence of the insert via PCR and sequencing, using an insert-specific forward primer (Myb5_10F for *M. l. variegatus* and Myb5_12F for *M. l. luteus*) and a reverse primer, att-R2, that binds to the recombination site at the 3'-end of the insert in recombined pEARLEYGATE vectors.

To exclude colonies with unrecombined entry vector, restriction endonuclease digests were performed as an additional diagnostic on plasmid purified from those colonies. Because it cuts both within the destination vector and within the insert, the HinDIII enzyme was used (Promega Corp., Madison, WI). Reactions were incubated for 60 minutes at 37ºC, then heat-inactivated for 15 minutes at 65ºC. Colonies that gave the expected digest pattern for recombined destination construct as well as the correct insert DNA sequence were chosen to proceed with this project.

Transformation into Agrobacterium

GV3101 electrocompetent *A. tumefaciens* cells, mixed with 1 µL isolated plasmid DNA (25-350 ng/µL) from each construct, were briefly exposed to a 2.5 kV, 200 ohm, 25 µF pulse using a BioRad® MicroPulser Electroporator (BioRad Laboratories, Hercules, CA, USA). The mixture was then immediately combined with 1 mL room-temperature LB media without antibiotics, incubated at 28ºC for 2-3 hours with shaking at 200 rpm., then plated on selective media. Putative transformants were tested for transgene insertion using a PCR screen with primers pEG-35S-attB1_F and att-R2 (Supplemental Table S1).

GFP-expressing plasmid for negative control

To screen for non-specific effects of transgene infiltration, the *A. tumefaciens*-compatible GFP expression plasmid pGFPGUSPlus was used as a negative control. pGFPGUSPlus was a gift from Claudia Vickers (Addgene plasmid # 64401; http://n2t.net/addgene:64401; RRID:Addgene_64401) (Vickers et al., 2007). Using the protocol in the previous section, the plasmid was transformed into *A. tumefaciens*.

Transient transformation

A video documenting our transformation methodology, adapted from Ding and Yuan (2016), is available upon request.

Agrobacterium colonies were PCR-screened to verify that they contained the desired transgene (pGFPGUSPlus, or *MYB5a* CDS from *M. l. luteus* or *M. l. variegatus*), and were then grown 16-24 hours in 5 mL LB (*Agrobacterium* recipe) at 28°C with appropriate antibiotics. The small culture was brought up to 50 mL with LB plus antibiotics and grown 12-16 hours at 28°C.

The 50-mL cultures were centrifuged in a Beckman-Coulter Allegra 25R temperature-controlled benchtop centrifuge (Beckman Coulter Inc, Brea, CA, USA) at 4ºC and 6,000 RCF for 15 minutes. The pellet was resuspended in a volume of 5% sucrose (w/v) solution equivalent to between one half and one time the original culture's volume. Resuspensions were adjusted, through dilution with the sucrose solution, to have the same optical density at 600 nm (OD_{600}) across all three transgene types within each trial, with an OD_{600} range of 1.6-1.9 across trials. Departing from Ding

and Yuan (2016), acetosyringone and Silwet L-77 were not included in the resuspension solution; omitting these reagents was proposed as a possible solution for leaf tissue damage previously observed in infiltrated *Mimulus lewisii* leaves (B. Ding, personal communication).

A B-D 1-mL slip tip disposable SubQ syringe (Becton, Dickinson and Company, Franklin Lakes, NJ, USA) with the needle removed was used to deliver *A. tumefaciens* cells to the leaves of young (1-3 months) *N. tabacum*. Using a gloved finger, the top of the leaf was held firmly while the underside of the leaf was injected with the syringe until the liquid had visibly spread past the site of injection. A volume of 100-200µL resuspended cells was injected per spot. The *M. l. luteus MYB5a* transgene and the *M. l. variegatus MYB5a* transgene were infiltrated in pairs, alternating with each leaf which transgene was injected into the left versus the right side of the leaf. A smaller number of negative controls was performed, with pGFPGUSPlus infiltrations approximately evenly distributed between the two sides of other leaves on the same plants.

Image acquisition and preparation

Leaves were imaged starting three days after infiltration, since Li et. al. (2009) reported that maximum expression of *Agrobacterium*-delivered transgenes occurs 3 days after infiltration. Because accumulation of visible gene product (anthocyanin) continued for several days after infiltration in some samples, leaves were imaged until a maximum of twelve days after infiltration. Digital photographs of infected leaves were then taken in a dark room with a Nikon D3500 DSLR camera with 18-55mm lens. The camera was fixed on a stand and the leaf was illuminated by a Sylvania Ceramic Metal Halide bulb, which exceeds 15,000 lumens, as the light source. All exposures produced both RAW and jpeg images, with RAW images used for the analysis and jpeg images used for interoperability with image annotation software. VGG Image Annotator was

used to demarcate the regions of interest covering the extent of the infiltrated leaf tissue and the center of each injection site.

Image analysis

S_{green}, which is the strength of the green channel relative to the total of all three color channels, was previously found to correlate highly (R^2 >= 0.63, p<.001) with anthocyanin concentration across a range of taxa and plant tissues (del Valle et. al. 2018). This is because anthocyanin absorbs light in the green region of the visible spectrum. The index, S_{green}, is given by:

$$S_{green} = N_{green} / (N_{green} + N_{blue} + N_{red})$$

where N is the intensity value for the green, blue, or red color channel (del Valle et al. 2018).

A custom Python program imported the RAW image files for processing. The Python program used a modified version of the MacDuff color chart detection algorithm (https://github.com/mathandy/python-macduff-colorchecker-detector) to automatically detect the panels of known broad-spectrum reflectance values on a reference color chart. Image pixel values were converted into normalized reflectance values based on a linear fit of the red, green, and blue signal strengths in those panels of known reflectance. The program then averages the relative greenness (S_{green}) value over all pixels of the annotated region of interest minus a circular region 20 pixels in radius at the injection site, which typically exhibited tissue damage from the injection syringe. This yielded a single S_{green} value for each sample.

S_{green} values were analyzed in R 4.1.2 using one-way ANOVAs, followed by Tukey post hoc tests when differences across treatments were discovered. A substantial number of leaves infiltrated

with *MYB5a* did not produce visible quantities of red pigmentation. These were categorized as "no visible pigment" if their S_{green} values showed them to have equal or lower amounts of red pigmentation than the average of all the negative controls; this categorization corresponded well with a "by-eye" assessment. Data were analyzed both with and without these apparently-unsuccessful infiltrations. Rates of success were compared between the *luteus* and *variegatus* transgenes using a X^2 contingency test in R 4.1.2.

Data availability

A detailed transient-transformation methods video is available upon request. Images of all leaves analyzed are linked as Supplemental Figure S8.A, S8.B, and S8.C in the Supplemental Data. *MYB5a* sequences from the exon 1-2-4 splice variants of *M. l. luteus* and *M. l. variegatus* have been previously published: https://www.ncbi.nlm.nih.gov/nuccore/MT361119.1 (*M. l. luteus*) and https://www.ncbi.nlm.nih.gov/nuccore/2019733960 *(M. l. variegatus*). Code for image analysis is available at https://github.com/WhitmanOptiLab/PigmentSpotting.

Results

Two sites in MYB5a *are occasionally sequenced as guanine rather than adenine*

The locations of two putatively edited sites, in exon 4 of *M. l. variegatus MYB5a*, are shown in Figure 2, along with chromatograms from the "AA" variant versus the "GG" variant from our initial, fortuitous discovery of the sequence difference. The novel "GG" variant was found in two different sequencing reactions, originating from two cDNA synthesis reactions from a single mRNA extraction of *M. l. variegatus* young bud outer-petal tissue.

469 *The "GG" allele of* MYB5a *from* M. l. variegatus *is not genomically encoded*

470

471 Cloning *MYB5a* gDNA from a *variegatus x luteus* F1 hybrid yielded 29 colonies containing a
472 *MYB* sequence. Of these, 13 contained the "AA" variant of the *M. l. variegatus* allele. The
473 remaining 16 contained the *M. l. luteus* allele. The "GG" variant was not discovered in these
474 genomic DNA samples.

475

476 Cloning *MYB5a* gDNA from a highly inbred line of *M. l. variegatus* yielded 37 colonies
477 containing a *MYB* sequence. All of these were the "AA" variant of *M. l. variegatus MYB5a*. The
478 "GG" variant was not discovered in these genomic DNA samples. Sample PCR colony screens,
479 from both F1 hybrid gDNA and *M. l. variegatus* gDNA, are shown in Supplemental Figure S6.

480

481 After collecting new floral bud tissues, and cloning and sequencing *MYB5a* cDNA from them, we
482 identified one additional colony containing a G at the edited site encompassed by our primers
483 (Table 1). As before, the variant was obtained from the petal lobes ("outer petal") of *M. l.*
484 *variegatus*. The other 29 *M. l. variegatus* colonies contained the "AA" variant. In *M. l. variegatus,*
485 only the exon 1-2-4 splice variant was recovered, as expected based on the utilization of
486 primers Myb5_64F and Myb5_57R (Supplemental Figure S5). These same primers were,
487 however, competent to amplify both 1-2-3 and 1-2-4 splice variants from *M. l. luteus*, and they
488 did. We found 28 colonies containing the exon 1-2-4 splice variant of *M. l. luteus MYB5a*, and
489 13 containing the exon 1-2-3 splice variant, with both splice variants appearing in both inner and
490 outer petal tissue (Table 1).

491

492 Recovering *M. l. luteus MYB5a* sequence from outer petal tissue was unexpected, and may
493 reflect imprecise separation of the two tissue types during floral bud dissection. The finding is

494 consistent with RT-PCR of *MYB5a* from our four cDNA samples, which indicated some
495 expression of the gene in the *M. l. luteus* outer petal sample (Supplemental Figure S7).
496
497
498 **Table 1. Sequencing *MYB5a* cDNA from *M. l. luteus* and *M. l. variegatus* developing flower bud**
499 **tissue identifies splice variants in *M. l. luteus,* and sequence variants in *M. l. variegatus.*** "Inner
500 petal" corresponds to the nectar-guide-spotted throat region of the flower; "outer petal" corresponds to the
501 petal lobes.

MYB5a variant	*luteus* inner petal	*luteus* outer petal	*variegatus* inner petal	*variegatus* outer petal
Exons 1-2-4 with "A"	17	11	10	19
Exons 1-2-4 with "G"	-	-	-	1
Exons 1-2-3	10	3	-	-

502
503 *Infiltration of transgenes into* N. tabacum *leaves*
504 Of the 124 leaves that received paired infiltrations of the 1-2-4 splice variant of *MYB5a* (*M. l.*
505 *variegatus* on one side of the central vein, and *M. l. luteus* on the other), 26 were eliminated due
506 to tearing or inadvertent marking over the pigmented area. The remaining 98 were scored for
507 the presence of visible anthocyanin pigmentation, and also quantitatively analyzed for pigment
508 abundance. Of the 25 leaves infiltrated on each side of the midvein with pGFPGusPlus as a
509 negative control, five were eliminated due to tearing or marking errors and the remaining 20
510 leaves (40 infiltrations) were quantitatively analyzed for anthocyanin pigment abundance
511 (Supplemental Figure S8).
512
513 MYB5a *from both* M. l. luteus *and* M. l. variegatus *drives strong anthocyanin production*

Both *MYB5a* transgenes resulted in significantly redder leaf tissue, as indicated by lower S_{green} values, than did the negative control (Figure 3 and 4; $F(2, 233) = 12.43$; $p<0.0001$**)**. Surprisingly, the allele of *MYB5a* from the yellow-flowered *M. l. luteus* appeared to drive significantly greater anthocyanin production than the corresponding allele from the magenta-flowered *M. l. variegatus* (Tukey's post hoc test: p=0.0102).

Figure 3. *MYB5a* transgenes yielded a range of anthocyanin biosynthesis levels in *N. tabacum* leaves. In each image, the injection site is indicated with an arrow, labeled as n (negative control), l (*luteus* allele of *MYB5a*), or v (*variegatus* allele of *MYB5a*). Leaf photos for this figure were uniformly

525 brightened by 30% in Powerpoint to make anthocyanin pigmentation and injection sites easier to see,
526 although analyses were performed on un-brightened images.
527

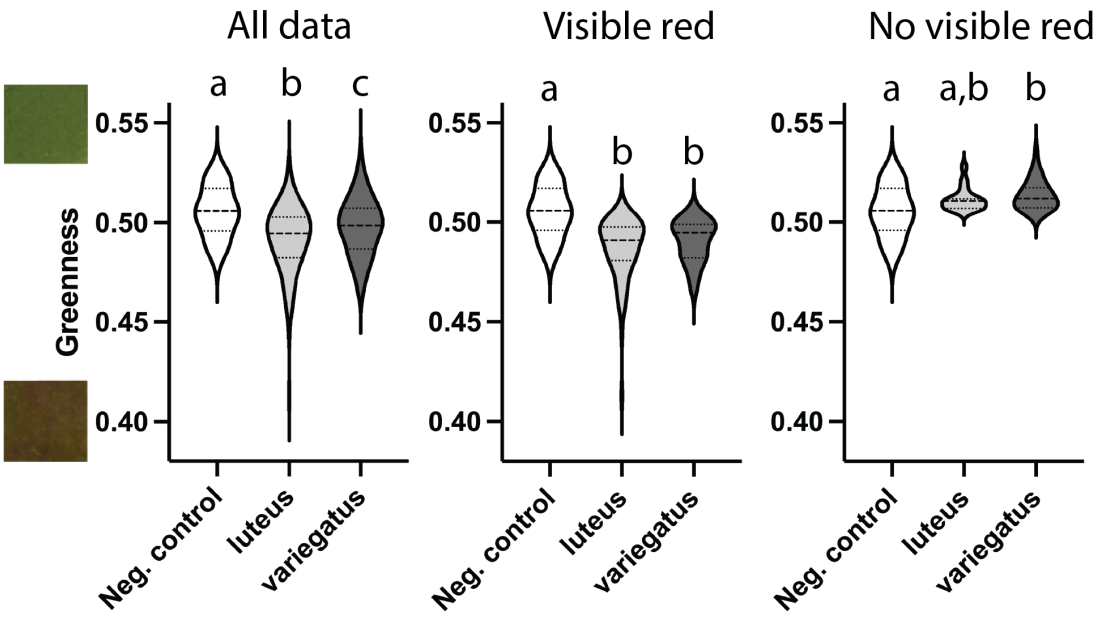

528

529 **Figure 4. *MYB5a* alleles from both the yellow-petaled *M. l. luteus* and the magenta-petaled *M. l.**
530 ***variegatus* drive production of red anthocyanin pigmentation in *N. tabacum* leaf tissue.** Left, data
531 from all samples. Center, pGFP negative control compared to only those *luteus* and *variegatus* samples
532 that produced visible amounts of red pigmentation. Right, pGFP negative control compared to those
533 *luteus* and *variegatus* samples that did not produce visible amounts of red pigmentation. Each graph is a
534 violin plot with the median shown as a dashed line and the first and third quartiles as dotted lines. On the
535 Y-axis, low values correspond to redder leaf tissue and high values correspond to greener tissue. Color
536 swatches on the Y-axis were taken from injection sites with S_{green} values of 0.53 and 0.41 respectively.
537 Swatches were taken from leaf photos that had been uniformly brightened by 30% in Powerpoint, to
538 maintain consistency with the previous figure, although analyses were performed on un-brightened
539 images. Letters a, b, and c are significance groupings at $p<0.05$.
540

541 However, this result may have been influenced by different rates of infiltration success, rather
542 than by different quantities of pigment produced in successful infiltration events. Overall, 79/98

543 *luteus* infiltrations, but only 67/98 *variegatus* infiltrations, resulted in the accumulation of visible
544 anthocyanin pigmentation in a tobacco leaf (Table 2). The difference in success rate between
545 the two alleles approached but did not reach statistical significance (χ^2 = 3.249, df = 1, p =
546 0.0715).
547
548 **Table 2. The *M. l. luteus* allele of *MYB5a* more often produced visible anthocyanin pigmentation in**
549 **tobacco leaves than did the *M. l. variegatus* allele, although the difference is not statistically**
550 **significant.** χ^2 = 3.249, df = 1, p = 0.0715.

Transgene	Leaves with visible anthocyanin	Leaves without visible anthocyanin
luteus MYB5a	79	19
variegatus MYB5a	67	31

551
552 To exclude possible effects of varying infiltration success, we analyzed pigment production only
553 from the infiltrations that produced visible amounts of leaf anthocyanin pigment (Figure 4 center
554 panel; F(2,183)=27.32, p<0.0001). In this subset of the data, the *luteus* and *variegatus*
555 transgenes were quite similar, and both drove significantly more anthocyanin pigmentation than
556 did the negative control (Tukey's post hoc: p<0.0001 for both *luteus* and *variegatus* compared to
557 the negative control).
558
559 In the excluded infiltrations **(**Figure 4 right panel; F(2,87)=6.731, p=0.00191), leaf tissues
560 containing the *luteus* and *variegatus* transgenes were statistically indistinguishable from each
561 other according to a Tukey's post hoc test, and slightly less red (higher S_{green} value) than the
562 negative control.
563

Discussion

When closely related taxa show phenotypic divergence, is the molecular mechanism a mutational difference in the protein-coding region of a gene, or in the noncoding, *cis*-regulatory region? We used transient transgenic assays to investigate this question for the MYB5a anthocyanin-activating transcription factor from two varieties of monkeyflower: the yellow-flowered *Mimulus luteus* var. *luteus*, which lacks anthocyanin pigment in its petal lobes, and the magenta-flowered *M. l. variegatus*, which recently evolved petal lobe anthocyanin via an unknown change within the *MYB5a* gene. Using quantitative image-analysis based methods, we report that the two protein-coding regions are functionally equivalent at driving the production of anthocyanin pigment in a heterologous tobacco-leaf system. Together with a previous finding that *MYB5a* is more strongly expressed in *M. l. variegatus* petal lobes than in its conspecific (Zheng et al. 2021), this result strongly indicates that *cis*-regulatory evolution is responsible for the recent gain of pigmentation in *M. l. variegatus*.

Improved tools for rapid transgenic assays in Mimulus

The success of the two *Mimulus* transgenes at activating anthocyanin production in *N. tabacum* is encouraging for future functional studies in *Mimulus*, though not unprecedented. One factor that can limit the ability of a MYB to function in a heterologous system is the availability of a functional bHLH co-factor. In some cases, co-expression of the focal MYB gene's native bHLH partner has been necessary for successful anthocyanin activation (Espley et al., 2009; Lin-Wang et al., 2010), but in other cases, anthocyanins have been induced in *N. tabacum* without also expressing bHLH from the same system (Fraser et. al., 2013). In one such study, Montefiori et. al. (2015) expressed *AcMyb110* from Kiwifruit (*Actinidia* sp., order Ericales) in *N.*

590 *tabacum* leaves and successfully stimulated anthocyanin production. They identified two
591 endogenous bHLH transcription factors in *N. tabacum*, NtJAF13 and NtAN1, that associated
592 with AcMYB110 to stimulate expression of anthocyanin biosynthetic pathway genes, and that
593 may also have interacted with the *Mimulus* MYB5a protein in our experiment.
594
595 One caveat to the finding of equivalence between the *luteus* and *variegatus* transgenes is that
596 the high levels of expression typically used in transgenic assays may obscure subtle differences
597 in protein function that only appear at lower concentrations (Koes et. al., 2005). It is possible that
598 other types of analyses could demonstrate a difference in molecular function between the two
599 alleles. Developing a more closely related species as a platform for functional tests would also be
600 beneficial. In our hands, preliminary tests with both *M. luteus* and congener *M. lewisii* resulted in
601 high levels of tissue death and damage, but the latter appears to have promise as a host for
602 transient transgenic assays (Ding and Yuan 2016).
603
604 Using *N. tabacum* for direct side-by-side comparison of *Agrobacterium*-delivered transgenes was
605 first reported by Van der Hoorn et. al. (2000). This strategy takes advantage of leaf symmetry and
606 the clearly delineated leaf sectors in *N. tabacum* to compare two genes side-by-side in an identical
607 biological background. Coupled with a nondestructive way to quantify the resulting phenotype, we
608 believe this remains an underutilized strategy for functional comparisons between genes.
609
610 *Possible A-to-I editing of mRNA*
611
612 In the process of building *MYB5a* overexpression transgenes, we discovered what appears to
613 be the first documented case, to our knowledge, of post-transcriptional editing in an
614 anthocyanin-related gene. Two sites within the *M. l. variegatus* allele are encoded as adenine in

615 the genome, yet occasionally produce mRNA sequences that read as a guanine in Sanger
616 sequencing.
617
618 Inosine is a guanine analog, most often created in cells by the deamination of adenine
619 (Srinivasan et al., 2021), that is reported as guanine in Sanger sequencing (Cattenoz et al.,
620 2013). Adenine-to-inosine (A-to-I) editing was first discovered in *Xenopus laevis* mRNA by Bass
621 and Weintraub (1988), and is abundant in metazoans (Cattenoz et al., 2013), with one study
622 predicting over 36,000 A-to-I editing sites in the human genome (Li et al., 2009).
623
624 Although A-to-I editing of mRNA transcripts does not yet appear to have been directly
625 investigated in plants, we hypothesize that the two new bases are in fact inosine, given that
626 inosine is reported as guanine by Sanger sequencing (Cattenoz et al., 2013). Nuclear A-to-I
627 post-transcriptional editing has been reported in plant tRNA (Delannoy et al., 2009; Karcher and
628 Bock 2009; Zhou et al., 2014), and the deaminase enzymes required for A-to-I editing have
629 been putatively discovered in *Arabidopsis thaliana* (Zhou et al., 2014). Though mRNA A-to-I
630 editing has not been described in plants, it is widespread across the domains of life, including
631 fungi (reviewed in Teichert 2018), animals (reviewed in Knoop 2011), and bacteria (first reported
632 by Bar-Yaacov et al., 2017).
633
634 In contrast, reports of A-to-G editing in plants appear to be based solely on sequencing-based
635 approaches that would report inosines incorrectly as guanines (Pan et al., 2022), with A-to-I
636 editing apparently first proposed by Meng et al. (2010) on the basis of A-to-"G" mRNA editing
637 discovered by sequencing plant transcriptomes. True A-to-G editing does not appear to be a
638 verified biological phenomenon in any taxon. We therefore consider A-to-G editing to be less
639 likely than A-to-I editing in our study.
640

641 A variety of methods exist for confirming A-to-I editing, including chromatographic approaches
642 (Wolf et al., 2002; Chan et al., 2010) and “inosine chemical erasing” (ICE)-Seq (Sakurai et al.,
643 2010). However, A-to-I editing is commonly detected and quantified by the simple method used
644 here, in which reverse transcription and sequencing of mRNA reveals unexpected “guanines” in
645 some proportion of transcripts (e.g. Gu et al., 2012).
646
647 When inosine is present in tRNA, it can pair promiscuously with A, C, or U. In mRNA transcripts,
648 in contrast, it is translated as though it were guanine (Srinivasan et al. 2021). Regardless of
649 whether the edited bases result in guanine or inosine, then, they are likely to be interpreted by
650 the translational machinery of the cell as guanine. In the *M. l. variegatus* allele of *MYB5a*, both
651 edited sites would result in an amino acid change: from asparagine to serine at nucleotide
652 position 584, and from glutamic acid to glycine at position 686.
653
654 How conservative are these changes? One metric is Grantham’s Distance, based on
655 composition, polarity and molecular volume (Grantham 1974). Using this metric, amino acid
656 pairs have similarity scores ranging from 5 for the highly similar leucine-isoleucine pair to a
657 maximum of 215 for cysteine-tryptophan. The first putative editing site reported here
658 (asparagine-serine, both of which have polar side chains) has a modest Grantham’s Distance of
659 46. The putative glutamic acid to glycine substitution - replacing a negatively charged side chain
660 with a single hydrogen - has a larger Grantham’s Distance of 98. The implications for MYB5a
661 protein folding and function are, however, unknown. Overall, the mechanisms for A-to-I (or A-to-
662 G) editing in plant mRNAs, and their functional impacts, comprise a barely-explored area within
663 plant molecular biology, which seems likely to yield new discoveries upon further investigation.
664 Nanopore native RNA sequencing methods, recently used by Nguyen et. al. (2022) to globally
665 identify inosine in human, mouse, and *Xenopus* transcriptomes, might be applied fruitfully to
666 plant transcriptomes with the same aim.

667

668

669 **Conclusions**

670

671 *Mimulus luteus* var. *luteus* and *M. l. variegatus* differ strikingly in floral phenotype, thanks to a
672 derived loss of yellow carotenoid pigment and gain of magenta cyanidin pigment in the latter.
673 The expansion of cyanidin to the petal lobes of *M. l. variegatus* has previously been tracked to
674 the *MYB5a* transcription factor gene, for which the patterns of petal expression correlate well
675 with the presence versus absence of cyanidin pigment. Here, we use transient transgenics
676 coupled with quantitative digital image analysis to show that the protein-coding regions of
677 *MYB5a* are functionally indistinguishable between the taxa, when tested in the heterologous
678 *Nicotiana tabacum* system. This finding adds further support to the hypothesis that evolution in
679 *cis* to *MYB5a* is the molecular mechanism for the gain of this novel anthocyanin trait in *M. l.*
680 *variegatus.*

681

682 We additionally report the discovery of what appears to be post-transcriptional mRNA editing.
683 The edits are reported as A-to-G by Sanger sequencing, but we argue that A-to-I editing is more
684 likely based on what is known about RNA editing in plants and other organisms. Overall, our
685 work highlights the utility of floral diversification for identifying the molecular mechanisms of
686 evolution, as well as the scope for continued new discoveries in the realm of plant molecular
687 genetics.

688

689 **Acknowledgements and Funding**

690

691 The authors thank N. Forsthoefel, B. Ding, and Y.-W. Yuan for assistance with and advice on
692 the transgenic techniques. We thank D. Vernon, B. Moss, J. Puzey, and their students for

693 discussion of some of the results presented here. AMC was supported by NSF-DEB-1655311,
694 NSF-DEB-1754075, and NSF-IOS-2031272. AEP was additionally supported by a Whitman
695 College Abshire Award for undergraduate research.

696

697 **References**

698

699 Barker, W. R., G. L. Nesom, P. M. Beardsley, and N. S. Fraga. 2012. A taxonomic
700 conspectus of Phrymaceae: a narrowed circumscription for Mimulus, new and
701 resurrected genera, and new names and combinations. Phytoneuron 39:1–60.
702 Bar-Yaacov, D., E. Mordret, R. Towers, T. Biniashvili, C. Soyris, S. Schwartz, O. Dahan,
703 and Y. Pilpel. 2017. RNA editing in bacteria recodes multiple proteins and regulates an
704 evolutionarily conserved toxin-antitoxin system. Genome Res. 27:1696–1703.
705 Bass, B. L., and H. Weintraub. 1988. An unwinding activity that covalently modifies its
706 double-stranded RNA substrate. Cell 55:1089–1098.
707 Beardsley, P. M., and R. G. Olmstead. 2002. Redefining Phrymaceae: the placement of
708 *Mimulus* , tribe Mimuleae, and *Phryma*. Am. J. Bot. 89:1093–1102.
709 Cattenoz, P. B., R. J. Taft, E. Westhof, and J. S. Mattick. 2013. Transcriptome-wide
710 identification of A > I RNA editing sites by inosine specific cleavage. RNA 19:257–270.
711 Chan, C. T. Y., M. Dyavaiah, M. S. DeMott, K. Taghizadeh, P. C. Dedon, and T. J. Begley.
712 2010. A Quantitative Systems Approach Reveals Dynamic Control of tRNA
713 Modifications during Cellular Stress. PLoS Genet 6:e1001247.
714 Cooley, A. M., G. Carvallo, and J. H. Willis. 2008. Is Floral Diversification Associated with
715 Pollinator Divergence? Flower Shape, Flower Colour and Pollinator Preference in
716 Chilean Mimulus. Annals of Botany 101:641–650.

717 Cooley, A. M., J. L. Modliszewski, M. L. Rommel, and J. H. Willis. 2011. Gene Duplication
718 in Mimulus Underlies Parallel Floral Evolution via Independent trans-Regulatory
719 Changes. Current Biology 21:700–704.
720 Cooley, A. M., and J. H. Willis. 2009. Genetic divergence causes parallel evolution of flower
721 color in Chilean *Mimulus*. New Phytologist 183:729–739.
722 Davies, K. M., N. W. Albert, and K. E. Schwinn. 2012. From landing lights to mimicry: the
723 molecular regulation of flower colouration and mechanisms for pigmentation patterning.
724 Functional Plant Biol. 39:619.
725 del Valle, J. C., A. Gallardo-López, M. L. Buide, J. B. Whittall, and E. Narbona. 2018. Digital
726 photography provides a fast, reliable, and noninvasive method to estimate anthocyanin
727 pigment concentration in reproductive and vegetative plant tissues. Ecol Evol 8:3064–
728 3076.
729 Delannoy, E., M. Le Ret, E. Faivre-Nitschke, G. M. Estavillo, M. Bergdoll, N. L. Taylor, B. J.
730 Pogson, I. Small, P. Imbault, and J. M. Gualberto. 2009. *Arabidopsis* tRNA Adenosine
731 Deaminase Arginine Edits the Wobble Nucleotide of Chloroplast tRNAArg(ACG) and Is
732 Essential for Efficient Chloroplast Translation. The Plant Cell 21:2058–2071.
733 Ding, B., and Y.-W. Yuan. 2016. Testing the utility of fluorescent proteins in Mimulus lewisii
734 by an Agrobacterium-mediated transient assay. Plant Cell Rep 35:771–777.
735 Dubos, C., R. Stracke, E. Grotewold, B. Weisshaar, C. Martin, and L. Lepiniec. 2010. MYB
736 transcription factors in Arabidopsis. Trends in Plant Science 15:573–581.
737 Durbin, M. 2003. Genes that determine flower color: the role of regulatory changes in the
738 evolution of phenotypic adaptations. Molecular Phylogenetics and Evolution 29:507–
739 518.
740 Edger, P. P., R. Smith, M. R. McKain, A. M. Cooley, M. Vallejo-Marin, Y. Yuan, A. J.
741 Bewick, L. Ji, A. E. Platts, M. J. Bowman, K. L. Childs, J. D. Washburn, R. J. Schmitz,
742 G. D. Smith, J. C. Pires, and J. R. Puzey. 2017. Subgenome Dominance in an

743 Interspecific Hybrid, Synthetic Allopolyploid, and a 140-Year-Old Naturally Established
744 Neo-Allopolyploid Monkeyflower. Plant Cell 29:2150–2167.
745 Espley, R. V., C. Brendolise, D. Chagné, S. Kutty-Amma, S. Green, R. Volz, J. Putterill, H.
746 J. Schouten, S. E. Gardiner, R. P. Hellens, and A. C. Allan. 2009. Multiple Repeats of a
747 Promoter Segment Causes Transcription Factor Autoregulation in Red Apples. The
748 Plant Cell 21:168–183.
749 Feller, A., K. Machemer, E. L. Braun, and E. Grotewold. 2011. Evolutionary and
750 comparative analysis of MYB and bHLH plant transcription factors: Plant MYB and
751 bHLH factors. The Plant Journal 66:94–116.
752 Fraser, L. G., A. G. Seal, M. Montefiori, T. K. McGhie, G. K. Tsang, P. M. Datson, E.
753 Hilario, H. E. Marsh, J. K. Dunn, R. P. Hellens, K. M. Davies, M. A. McNeilage, H. N. D.
754 Silva, and A. C. Allan. 2013. An R2R3 MYB transcription factor determines red petal
755 colour in an Actinidia (kiwifruit) hybrid population. BMC Genomics 14:28.
756 Grantham, R. 1974. Amino Acid Difference Formula to Help Explain Protein Evolution.
757 Science 185:862–864.
758 Grotewold, E. 2006. The genetics and biochemistry of floral pigments. Annu. Rev. Plant
759 Biol. 57:761–780.
760 Gu, T., F. W. Buaas, A. K. Simons, C. L. Ackert-Bicknell, R. E. Braun, and M. A. Hibbs.
761 2012. Canonical A-to-I and C-to-U RNA Editing Is Enriched at 3′UTRs and microRNA
762 Target Sites in Multiple Mouse Tissues. PLoS ONE 7:e33720.
763 Hoekstra, H. E., and J. A. Coyne. 2007. The Locus of Evolution: Evo Devo and the
764 Genetics of Adaptation. Evolution 61:995–1016.
765 Kapila, J., R. De Rycke, M. Van Montagu, and G. Angenon. 1997. An Agrobacterium-
766 mediated transient gene expression system for intact leaves. Plant Science 122:101–
767 108.

768 Karcher, D., and R. Bock. 2009. Identification of the chloroplast adenosine-to-inosine tRNA
769 editing enzyme. RNA 15:1251–1257.
770 Knoop, V. 2011. When you can't trust the DNA: RNA editing changes transcript sequences.
771 Cell. Mol. Life Sci. 68:567–586.
772 Koes, R., W. Verweij, and F. Quattrocchio. 2005. Flavonoids: a colorful model for the
773 regulation and evolution of biochemical pathways. Trends in Plant Science 10:236–
774 242.
775 LaFountain, A. M., and Y. Yuan. 2021. Repressors of anthocyanin biosynthesis. New
776 Phytol 231:933–949.
777 Li, C., W. Yu, J. Xu, X. Lu, and Y. Liu. 2022. Anthocyanin Biosynthesis Induced by MYB
778 Transcription Factors in Plants. IJMS 23:11701.
779 Li, J. B., E. Y. Levanon, J.-K. Yoon, J. Aach, B. Xie, E. LeProust, K. Zhang, Y. Gao, and G.
780 M. Church. 2009a. Genome-Wide Identification of Human RNA Editing Sites by
781 Parallel DNA Capturing and Sequencing. Science 324:1210–1213.
782 Li, J.-F., E. Park, A. G. von Arnim, and A. Nebenführ. 2009b. The FAST technique: a
783 simplified Agrobacterium-based transformation method for transient gene expression
784 analysis in seedlings of Arabidopsis and other plant species. Plant Methods 5:6.
785 Lin-Wang, K., K. Bolitho, K. Grafton, A. Kortstee, S. Karunairetnam, T. K. McGhie, R. V.
786 Espley, R. P. Hellens, and A. C. Allan. 2010. An R2R3 MYB transcription factor
787 associated with regulation of the anthocyanin biosynthetic pathway in Rosaceae. BMC
788 Plant Biol 10:50.
789 Lowry, D. B., J. M. Sobel, A. L. Angert, T. Ashman, R. L. Baker, B. K. Blackman, Y.
790 Brandvain, K. J. R. P. Byers, A. M. Cooley, J. M. Coughlan, M. R. Dudash, C. B.
791 Fenster, K. G. Ferris, L. Fishman, J. Friedman, D. L. Grossenbacher, L. M. Holeski, C.
792 T. Ivey, K. M. Kay, V. A. Koelling, N. J. Kooyers, C. J. Murren, C. D. Muir, T. C. Nelson,
793 M. L. Peterson, J. R. Puzey, M. C. Rotter, J. R. Seemann, J. P. Sexton, S. N. Sheth,

M. A. Streisfeld, A. L. Sweigart, A. D. Twyford, M. Vallejo-Marín, J. H. Willis, K. M. Wright, C. A. Wu, and Y. Yuan. 2019. The case for the continued use of the genus name *Mimulus* for all monkeyflowers. TAXON 68:617–623.

Meng, Y., D. Chen, Y. Jin, C. Mao, P. Wu, and M. Chen. 2010. RNA editing of nuclear transcripts in Arabidopsis thaliana. BMC Genomics 11:S12.

Montefiori, M., C. Brendolise, A. P. Dare, K. Lin-Wang, K. M. Davies, R. P. Hellens, and A. C. Allan. 2015. In the Solanaceae, a hierarchy of bHLHs confer distinct target specificity to the anthocyanin regulatory complex. Journal of Experimental Botany 66:1427–1436.

Nguyen, T. A., J. W. J. Heng, P. Kaewsapsak, E. P. L. Kok, D. Stanojević, H. Liu, A. Cardilla, A. Praditya, Z. Yi, M. Lin, J. G. A. Aw, Y. Y. Ho, K. L. E. Peh, Y. Wang, Q. Zhong, J. Heraud-Farlow, S. Xue, B. Reversade, C. Walkley, Y. S. Ho, M. Šikić, Y. Wan, and M. H. Tan. 2022. Direct identification of A-to-I editing sites with nanopore native RNA sequencing. Nat Methods 19:833–844.

Pan, Y., M. Li, J. Huang, W. Pan, T. Shi, Q. Guo, G. Yang, and X. Nie. 2022. Genome-Wide Identification and Characterization of RNA/DNA Differences Associated with Drought Response in Wheat. IJMS 23:1405.

Puzey, J. R., J. H. Willis, and J. K. Kelly. 2017. Population structure and local selection yield high genomic variation in *Mimulus guttatus*. Mol Ecol 26:519–535.

Quattrocchio, F., W. Verweij, A. Kroon, C. Spelt, J. Mol, and R. Koes. 2006. PH4 of Petunia Is an R2R3 MYB Protein That Activates Vacuolar Acidification through Interactions with Basic-Helix-Loop-Helix Transcription Factors of the Anthocyanin Pathway. The Plant Cell 18:1274–1291.

Sakurai, M., T. Yano, H. Kawabata, H. Ueda, and T. Suzuki. 2010. Inosine cyanoethylation identifies A-to-I RNA editing sites in the human transcriptome. Nat Chem Biol 6:733–740.

820 Schöb, H., C. Kunz, and F. Meins. 1997. Silencing of transgenes introduced into leaves by
821 agroinfiltration: a simple, rapid method for investigating sequence requirements for
822 gene silencing. Mol Gen Genet 256:581–585.
823 Sobel, J. M., and M. A. Streisfeld. 2013. Flower color as a model system for studies of plant
824 evo-devo. Front. Plant Sci. 4.
825 Sparkes, I. A., J. Runions, A. Kearns, and C. Hawes. 2006. Rapid, transient expression of
826 fluorescent fusion proteins in tobacco plants and generation of stably transformed
827 plants. Nat Protoc 1:2019–2025.
828 Srinivasan, S., A. G. Torres, and L. Ribas de Pouplana. 2021. Inosine in Biology and
829 Disease. Genes 12:600.
830 Stern, D. L., and V. Orgogozo. 2008. The Loci of Evolution: How Predictable Is Genetic
831 Evolution? Evolution 62:2155–2177.
832 Stracke, R., M. Werber, and B. Weisshaar. 2001. The R2R3-MYB gene family in
833 Arabidopsis thaliana. Current Opinion in Plant Biology 4:447–456.
834 Streisfeld, M. A., and M. D. Rausher. 2011. Population genetics, pleiotropy, and the
835 preferential fixation of mutations during adaptive evolution. Evolution 65:629–642.
836 Teichert, I. 2018. Adenosine to inosine mRNA editing in fungi and how it may relate to
837 fungal pathogenesis. PLoS Pathog 14:e1007231.
838 Tian, J., J. Zhang, Z. Han, T. Song, J. Li, Y. Wang, and Y. Yao. 2017. McMYB12
839 Transcription Factors Co-regulate Proanthocyanidin and Anthocyanin Biosynthesis in
840 Malus Crabapple. Sci Rep 7:43715.
841 Wittkopp, P. J., B. K. Haerum, and A. G. Clark. 2008. Regulatory changes underlying
842 expression differences within and between Drosophila species. Nat Genet 40:346–350.
843 Wolf, J. 2002. tadA, an essential tRNA-specific adenosine deaminase from Escherichia coli.
844 The EMBO Journal 21:3841–3851.

Wray, G. A. 2007. The evolutionary significance of cis-regulatory mutations. Nat Rev Genet 8:206–216.

Wu, C. A., D. B. Lowry, A. M. Cooley, K. M. Wright, Y. W. Lee, and J. H. Willis. 2008. Mimulus is an emerging model system for the integration of ecological and genomic studies. Heredity 100:220–230.

Yang, Y., R. Li, and M. Qi. 2000. In vivo analysis of plant promoters and transcription factors by agroinfiltration of tobacco leaves. Plant J 22:543–551.

Yuan, Y. 2019. Monkeyflowers (*Mimulus*): new model for plant developmental genetics and evo-devo. New Phytol 222:694–700.

Yuan, Y.-W., K. J. Byers, and H. Bradshaw. 2013a. The genetic control of flower–pollinator specificity. Current Opinion in Plant Biology 16:422–428.

Yuan, Y.-W., J. M. Sagawa, R. C. Young, B. J. Christensen, and H. D. Bradshaw. 2013b. Genetic Dissection of a Major Anthocyanin QTL Contributing to Pollinator-Mediated Reproductive Isolation Between Sister Species of *Mimulus*. Genetics 194:255–263.

Zheng, X., K. Om, K. A. Stanton, D. Thomas, P. A. Cheng, A. Eggert, E. Simmons, Y.-W. Yuan, G. D. Conradi Smith, J. R. Puzey, and A. M. Cooley. 2021. The regulatory network for petal anthocyanin pigmentation is shaped by the MYB5a/NEGAN transcription factor in *Mimulus*. Genetics 217:iyaa036.

Zhou, W., D. Karcher, and R. Bock. 2014. Identification of Enzymes for Adenosine-to-Inosine Editing and Discovery of Cytidine-to-Uridine Editing in Nucleus-Encoded Transfer RNAs of Arabidopsis. Plant Physiol. 166:1985–1997.

Supplemental tables

871 **Table S1.** Primers used. F and R in primer names indicate forward and reverse primer
872 directions with respect to the direction of transcription. *MYB5a* primers bind to both *M. l.*
873 *variegatus* and *M. l. luteus* alleles unless otherwise noted.

Primer ID	Sequence (5' to 3')	Target	Notes
att-R2	CACCACTTTGTACAAGAAAGCTG	pEARLEYGATE vector	
cacc_10F	CACCTTGCAGAGCATGGAAAACAC	MYB5a, end of 5'UTR through beginning of coding sequence	"cacc" tag enables directional cloning into entry vector
GAPDH_1F	TTGAAGGGAATCTTGGGCTA	GAPDH	used as a positive control
GAPDH_2R	CATTTGACGTACCATAAACGAGT	GAPDH	used as a positive control
M13F(-20)	GTAAAACGACGGCCAGT	pENTR entry vector	
M13R(-24)	AACAGCTATGACCATG	pENTR entry vector	
Myb5_10F	TTGCAGAGCATGGAAAACAC	MYB5a, end of 5'UTR through beginning of coding sequence	
Myb5_12F	TGTAGGTGTAAGAAAAGGTGCAT	Beginning of MYB5a Exon 1, luteus allele only	
Myb5_53R	TTAATTAGGCCCCAGTAGGC	End of MYB5a Exon 4, variegatus allele only	includes stop codon

Myb5_57R	CCATCTTCTGTCGTCGTAGTTTC	MYB5a Exon 4	can bind exon 3, though with 2 mismatches
Myb5_64F	GACGGCGGCGAAATTACT	MYB5a Exon 4	also binds exon 3, in luteus only
Myb5_69R	ATTAGGCCCCAGTAGGC	End of MYB5a Exon 4, variegatus allele only	does not include stop codon
pEG-35S-attB1_F	ACGCTCGAGATCACAAGTTT	pEARLEYGATE vector	

874

875

876

877 **Supplemental figures**

878

879 ***Myb3a* is present and expressed in the yellow morph of *M. cupreus*, but *Myb2* does not**

880 **appear to be.**

881

882 A

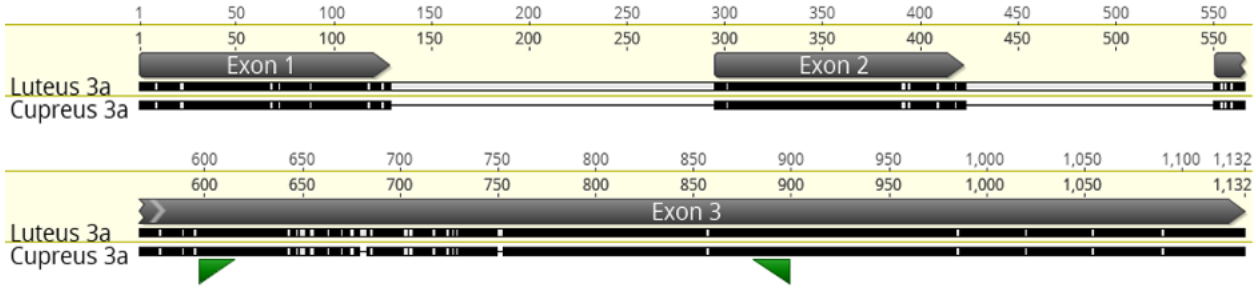

883

884 B

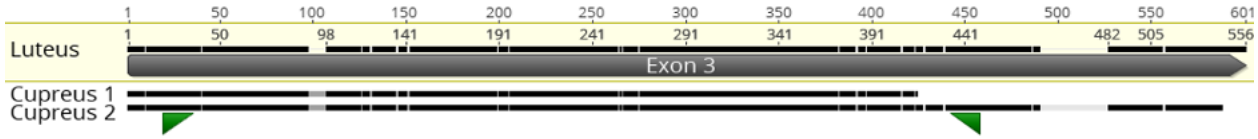

C

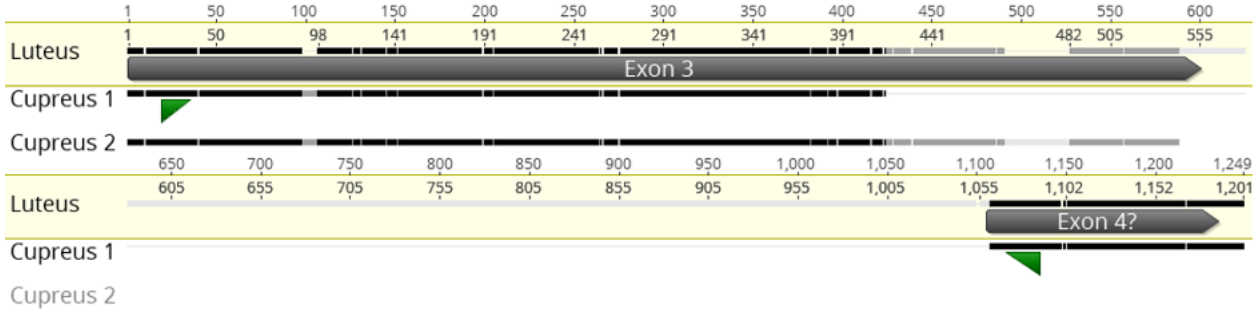

Figure S1. *Mimulus cupreus MYB3a* and *MYB2* transcripts aligned to *M. luteus* genomic sequence. A. *MYB3a*. Primers Myb2/3_1F and Myb3a_2R are shown in green. B. *MYB2*. Two *M. cupreus* transcripts were recovered from transcriptome sequence; the region in which they diverge is labeled as “Cupreus 1” and “Cupreus 2,” possibly corresponding to alternative splice variants. Primers Myb 2_1F and Myb 2b_5R shown in green. These primers are expected to amplify only transcript 2. C. The same *MYB2* transcripts with primers Myb 2_1F and Myb 2b_7R shown in green.

Figure S2. Primers Myb 2/3_1F and Myb 3a_2R were used to amplify a portion of *Myb3a* exon 3, encoding a transcription factor gene that is one of two candidates for the gain of petal

anthocyanin pigmentation in the orange-flowered morph of *M. cupreus* (Cooley et al., 2011). The recent loss of pigmentation in the rare yellow morph of *M. cupreus* also maps to the same region. A product of the expected length (300 bp) was amplified out of gDNA for both orange and yellow-flowered *M. cupreus.* The product was also amplified out of cDNA for both inner and outer petal tissue from both morphs, indicating that Myb 3a **is** expressed in all of these tissues.

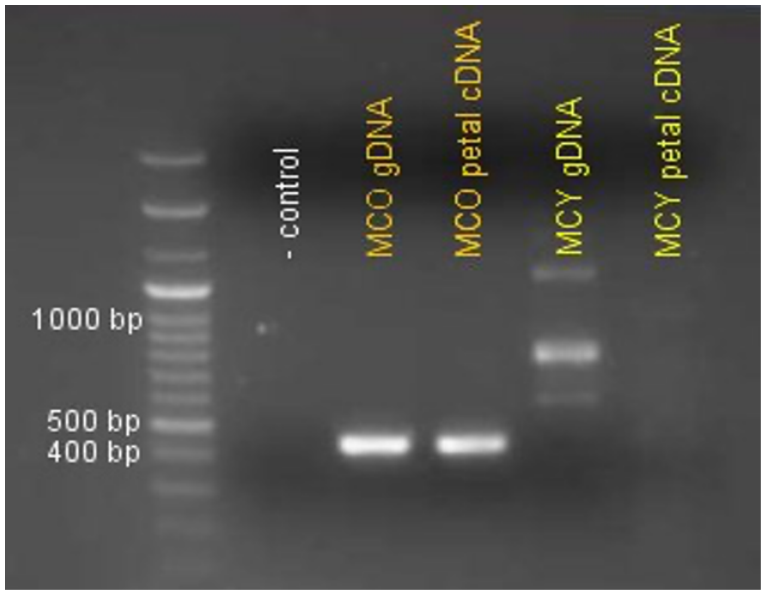

Figure S3. Primers Myb 2_1F and Myb 2b_5R were used to amplify a portion of *Myb2* transcript 2, exon 3, encoding a transcription factor gene that is the second of two candidates for the derived gain of petal anthocyanin pigmentation in the orange-flowered morph of *M. cupreus*, and the even more recent loss of petal anthocyanin in the rare yellow morph. A product of expected length (around 450 bp) was amplified out of orange-flowered *M. cupreus* gDNA. The product was also amplified out of cDNA from both inner and outer petal from orange-flowered *M. cupreus,* indicating that it is expressed in the orange morph. However, no product of the expected length was amplified out of yellow-flowered *M. cupreus* gDNA. Several longer products were amplified less brightly, and are likely due to nonspecific annealing. No product was seen in the yellow-flowered petal cDNA either.

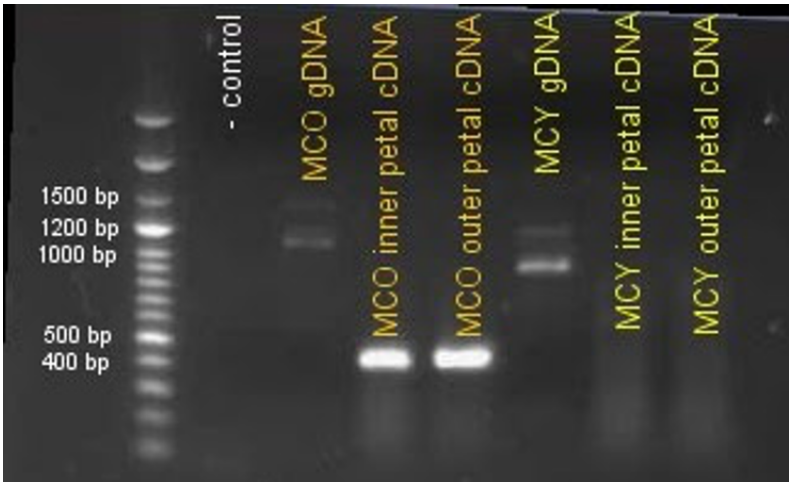

Figure S4. Primers Myb 2_1F and Myb 2b_7R were used to amplify a region of *Myb2* extending from the beginning of the third exon through the beginning of the predicted fourth exon. The expected length of the product spanning the third intron of Myb2 was estimated to be approximately 1050 bp based on the *M. luteus* genome. A PCR amplification done using standard Taq polymerase showed bands at 1050 bp and 1500 bp in orange-flowered *M. cupreus* gDNA and at 950 bp and 1300 bp in yellow-flowered *M. cupreus* gDNA. Amplification using long-amp Taq polymerase revealed that a 950 bp product was also present in gDNA from orange-flowered *M. cupreus*. Sequencing of these products showed that the 1050 bp fragment from orange *M. cupreus* corresponds to *Myb2*, while the two bands seen in yellow *M. cupreus* contain sequences with no resemblance to any anthocyanin-related Myb gene. In orange-flowered *M. cupreus* cDNA from both inner and outer petal, a product of approximately 430 bp was amplified. This indicates that the transcript is spliced as expected, and is expressed in inner and outer petal tissue of orange-flowered *M. cupreus.* No product was observed in the amplification out of yellow-flowered *M. cupreus* petal cDNA, indicating that the Myb 2b transcript is not expressed in yellow *M. cupreus* petals.

935

936

937

938

939

940

941

942

943

944

945

946

947

948

949 ***MYB5a* from both *M. l. luteus* and *M. l. variegatus* activates anthocyanin pigmentation**

951

952 **Figure S5.** Alleles of *MYB5a* from the yellow-petaled *M. l. luteus* (top sequence on each line)
953 and the magenta-petaled (anthocyanin-pigmented) *M. l. variegatus* (bottom sequence on each
954 line). Primers mentioned in the Methods are shown in dark green (forward primers) and light
955 green (reverse primers). Exons are marked in gray. Two putative A-to-I editing sites are marked
956 in yellow. Note that Subgroup 6, which is a hallmark of all known anthocyanin-activating R2R3
957 MYBs, is present in both taxa in exon 4 as the amino acid sequence RPRPRTF. In exon 3,
958 however, a frameshift mutation in *M. l. variegatus* eliminates this feature, making it unlikely that
959 the exon 1-2-3 splice variant of *M. l. variegatus* would be capable of anthocyanin activation.

960

961

962 A

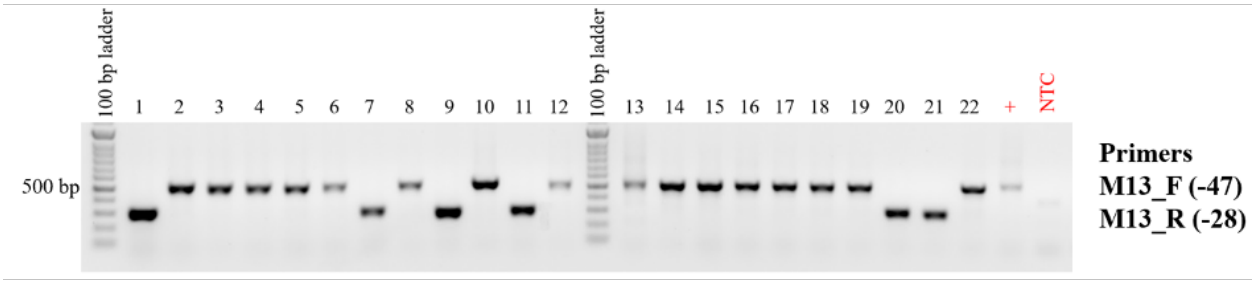

963

964 B

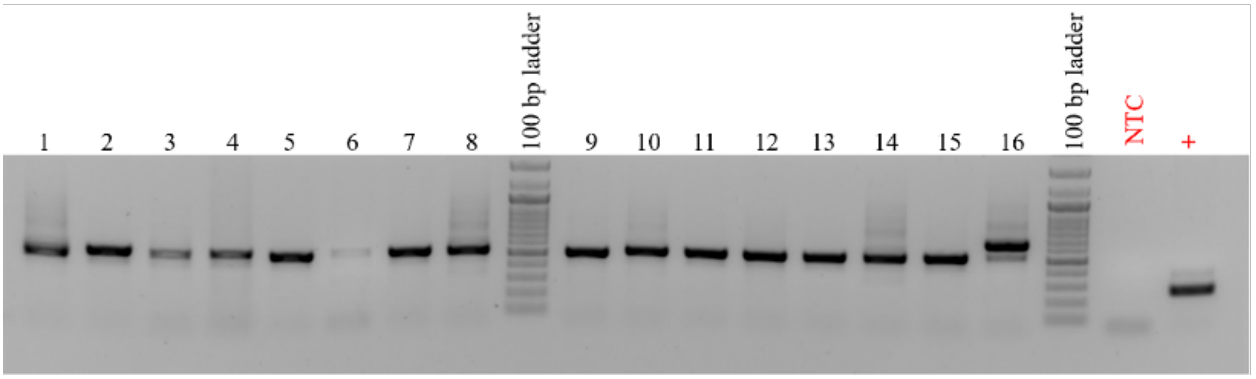

965

966 **Figure S6.** pGEM Cloning of an exon 4 fragment of *MYB5a*. A fragment containing the first
967 edited site was PCR-amplified using primers 64F-57R and cloned, and colonies were screened

968 for fragment insertion. Lanes with band size ~500 bp are colonies that contain the *MYB5a* exon
969 4 insert. Lanes with bands ~300 denote empty vectors. (A) Primers M13_F (-47) and M13_R (-
970 28) were used to screen white colonies from a pGEM cloning attempt with *M. l. variegatus* x *M.*
971 *l. luteus* F1 hybrid gDNA. 16 colonies appear to have taken up the MYB5 exon 4 insert. (B)
972 Primers M13_F (-47) and M13_R (-28) were used to screen white colonies from a pGEM
973 cloning attempt with Mlv gDNA. 15 colonies appear to have successfully taken up the insert.
974 The band at ~650bp most likely denotes a vector with a longer, incorrect insert.

975

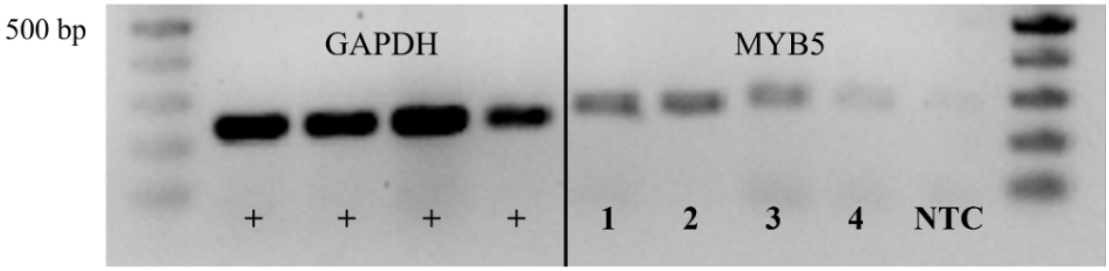

976

977 **Figure S7.** Relative expression of *MYB5a* in *M. l. variegatus* and *M. l. luteus*. Left: positive
978 control using GAPDH primers 1F-2R, on each of the samples shown on the right. Right: An
979 exon 4 fragment of *MYB5a* amplified using Myb5_64F and Myb5_57R from cDNA from *M. l.*
980 *variegatus* inner petal (1) and outer petal (2); the red-spotted *M. l. luteus* inner petal (3); and the
981 yellow *M. l. luteus* outer petal (4). NTC, No Template Control. All band sizes were as expected.

982

983

984 **Figure S8.** Leaf photos utilized in quantitative comparisons of anthocyanin production. Photos
985 excluded due to leaf damage are not included. A. pGFP negative controls, with two transgene
986 injections per leaf. B. Leaves for which the *M. l. variegatus MYB5a* exon 1-2-4 transgene was
987 injected on the left side of the leaf and the *M. l. luteus* allele on the right. C. Leaves for which the

988 *M. l. variegatus MYB5a* exon 1-2-4 transgene was injected on the right side of the leaf and the

989 *M. l. luteus* allele on the left. Files uploaded separately.

990

991

992